Colorimetric characterization of a 3D printer with a spectral model

Brittany D. Hensley and James A. Ferwerda, Munsell Color Science Laboratory, Rochester Institute of Technology, Rochester, New York, USA

Abstract

As 3D printing becomes an increasingly popular technology, knowledge of the processes employed by a printer becomes more important. In this paper, one particular printer, the Zcorp Spectrum Z510, is studied in terms of its color production. Two approaches to a spectral model are evaluated in terms of their ability to predict output colors of the printer based on input RGB values. The models and their performance are presented below.

Introduction

The popularity of 3D printers has been fueled by a growing interest of companies and businesses in rapid prototyping and rapid manufacturing. With the introduction of relatively low-cost 3D printer technologies, even individuals are now able to print 3D objects from CAD models [1]. Plastic, metal, ceramic, and even edible objects can be printed in various types of 3D printers. These objects can then be used as prototypes, final production, or unique customized products such as phone cases [2]. As the 3D printer market extends from engineers and scientists to small businesses and individual consumers, controlling the color properties of printed objects becomes increasingly important. Being able to measure and predict 3D-printed colors is an important part of the color 3D-printing workflow.

The technology of 3D printing was introduced in 1986 when Charles Hull patented a technique called stereolithography and developed the first practical 3D printer, the Stereolithography Apparatus [3]. However, the field of 3D printing did not begin to take shape until the 1990s and is still considered to be in the early stages. But it continues to grow and develop rapidly because of its many applications [3].

3D printers are considered additive manufacturing devices because they produce objects by adding material until the desired form is completed [1]. There are four dominant 3D printing technologies: stereolithography, selective laser sintering, fused deposition modeling, and powder/binder fusion. All four of these processes begin with a 3D CAD model that is "sliced" into layers by software and then printed layer by layer by the machine [4-6} The last of these technologies and the focus of this paper, powder/binder fusion, uses an inkjet like delivery system to deposit binder that fuses a plaster-like powder to produce layers. Of the four processes mentioned, this is the only one capable of printing full color objects through the use of colored binders [7].

Given the ability to print full colored objects, the desire to print particular colors is not far behind. Often users have a specific color in mind when they are modeling an object, and the ability to accurately produce that color in the final object is important. Therefore, just as with 2D color printing, we need to develop accurate color reproduction models for 3D color printers. A recent study by Stanic et al. was performed to assess the lightfastness of 3D color prints after accelerated exposure to a xenon-arc light source, but little has been done in the way of colorimetric characterization of 3D printers due, in part, to a lack of availability [8].

This paper explores two approaches to predicting the colors of 3D-printed objects from RGB color values using the Zcorp Spectrum Z-510 Printer. The first approach employs the use of the Yule-Nielsen Modified Neugebauer model. The second approach utilizes Principal Component Analysis on the spectral absorptance of printed samples.

Background

The Neugebauer model is based on the Murray-Davies that predicts output density from input dot area using the equation

$$\hat{R}_\lambda = a_t R_{\lambda,t} + (1 - a_t) R_{\lambda,s} \tag{1}$$

where a_t is the fractional dot area of the binder, $\hat{R}_\lambda$ is the predicted reflectance of the sample, $R_{\lambda,t}$ is the reflectance of the binder and $R_{\lambda,s}$ is the reflectance of the substrate [9]. This model uses measurements of only the solid binder and the substrate to determine the area coverage. The Murray-Davies model was extended by Neugebauer to include multiple colorants. This is done by incorporating the fractional area coverage of each colorant Eqn. (2).

$$\hat{R}_\lambda = \sum_{i=1 \rightarrow 2^k} w_i R_{\lambda,i,max} \tag{2}$$

In this equation k represents the number of binders used by the printer, *i* is the number of Neugebauer primaries, and w is the fractional area coverages of each colorant calculated according to Eqn. (3) [9].

$$w_i = \prod_{j=1 \rightarrow k} \begin{pmatrix} if\ ink\ j\ is\ in\ Primary\ i, then\ a_j \\ else, (1 - a_j) \end{pmatrix} \tag{3}$$

The Yule-Nielsen modification is introduced starting with the Murray-Davies model. This modification is intended to model the nonlinear relationship between measured and predicted reflectance. The assumption made by this model is that the predicted and measured reflectances do not match due to light penetration and scattering in the substrate [9]. Eqn. (4) shows the power function used to describe this relationship where n is a parameter used to account for light spreading in the substrate. This is the final form of the model used to model the 3D printer.

$$\hat{R}_\lambda = \left[\sum_{i=1 \rightarrow 2^k} w_i R_{\lambda,i,max}^{1/n} \right]^n \tag{4}$$

The second approach employs the transparent form of Kubelka-Munk equation shown in Eqn. (5). The reflectances used in this calculation are first corrected using the Saunderson correction shown in Eqn. (6).

$$K_{\lambda,mixture} = -0.5\ \ln\left(\frac{R_\lambda}{R_{\lambda,s}}\right) \tag{.5}$$

where K is the absorptance of the sample and R_s is the reflectance of the white powder or background [10].

$$R_{\lambda,i} = \frac{R_{\lambda,m}}{(1-K_1)(1-K_2)+K_2 R_{\lambda,m}} \qquad .6$$

The Saunderson correction is applied to account for intersurface reflections between the surface of the samples and air. The correction is based on the assumption that the refractive index of the binder and the powder have similar values and any difference is insignificant. The reflectance is corrected for refractive index discontinuity using the Saunderson equation for specular excluded conditions where K_1 and K_2 are assigned the theoretical values 0.04 and 0.6 and R_m is the measured reflectance [11].

The use of the transparent form of Kubelka-Munk theory has successfully been shown by Berns [11]. The use of the transparent form was chosen because the printing process employs the application of multiple concentration levels on a white substrate as well as the translucent appearance of the binder in its liquid form [12].

Zcorp Spectrum Z-510 Printer

The Printing Process

The Zcorp Spectrum Z510 3D printer is based on MIT's patented 3DP technology [7]. The printing process begins with a three-dimensional model built using a 3D CAD program. This three-dimensional model is sliced into cross sections between 0.0875 and 0.1 mm thick by the Zprint software [7]. These slices are then printed one on top of the other starting with the base.

The printer uses a white plaster powder and four different colored binders – cyan, magenta, yellow, and clear – to build the 3D objects.A flowchart of the printing process is shown in Fig. 1 [7]. As seen in this diagram, the printer mechanism includes a build envelope, a feed envelope, and a moving gantry that includes a roller and a print head. To begin the build process, the gantry moves left to right to pick up powder. The powder is deposited on the build envelope in a thin layer. The gantry then reverses direction and the print heads deposit the binder solutions which adhere the powder together. The build envelope then moves down, and the feed envelope moves up, and the process is repeated until all the necessary layers have been deposited to complete the 3D object.
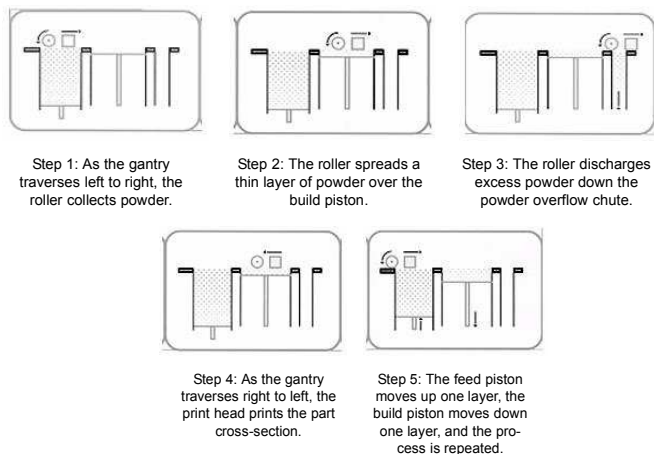

Step 1: As the gantry traverses left to right, the roller collects powder.

Step 2: The roller spreads a thin layer of powder over the build piston.

Step 3: The roller discharges excess powder down the powder overflow chute.

Step 4: As the gantry traverses right to left, the print head prints the part cross-section.

Step 5: The feed piston moves up one layer, the build piston moves down one layer, and the process is repeated.

Fig. 1. Flowchart of steps followed in the printing process of the ZCorp Z510 3D Printer [7].

The printer only colors the surface of the object, not the interior portions, which are white (the color of the powder fused using the clear binder). This is done because the colored binder is more expensive per volume than the clear binder [7].

Samples

To characterize the printer, a set of samples were created by printing 20 mm by 20 mm by 5 mm thick tiles of a variety of colors. Sample colors were specified by systematically varying the 0-255 RGB digital counts in the software. A total of 226 different color samples, including white, where a layer of clear binder is used, were printed. The samples included ramps of cyan, magenta, and yellow. A 5 x 5 x 5 factorial was also created using 33, 83, 133, 183, and 238 digital count values. The samples were printed using 0.100 mm layer thickness per printer pass and 100% binder saturation per the manufacturers recommendations [7].

Fig. 2 shows a magnified image of a yellow [225 225 0] tile. Note that the cyan, magenta, and yellow binders are all evident in this image as well as the white powder. The surface textures and specularities are also evident. This sample shows that there is contamination of other binders in the yellow samples beginning as early as the second purest sample in the color ramp. This was also seen with the cyan and magenta ramps.
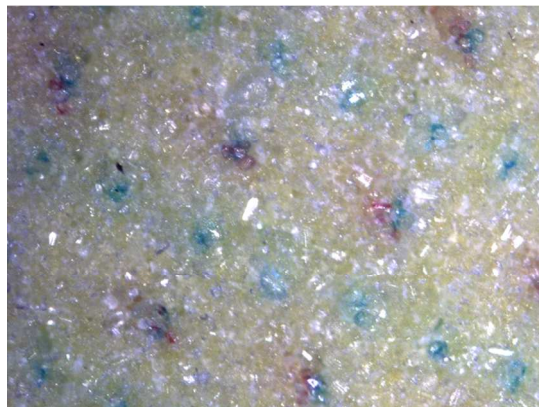

Fig. 2. Magnified image of a yellow tile that corresponds to the RGB digital counts [255 255 0]. All three colored binders are visible as well as surface textures and specularities.

Measuring Samples

The samples were measured using an XRite ColorEye 7000 with UV filter in place, and the specular component excluded. The ColorEye 7000 uses a pulsed Xenon light source and a D/8 diffuse optical geometry. The plots of the cyan, magenta, and yellow ramps are shown in Fig. 3. The UV filter was used to reduce the effects of fluorescence on the measured data. Because fluorescence depends on the light source, the models developed below only apply for the same illumination conditions (D65) as the condition used for taking measurements. When Fig. 3 is examined, a spectral curve stands out from the others. This is more prominent with the magenta and yellow samples. These curves are depicted with darker lines than the other curves. It is evident that the higher wavelength regions of these curves in question for the magenta and yellow are noticeably higher than the other curves. These curves correspond to the maximum color patches for each binder color. The curves may be different from the other samples because they correspond to the only samples in each ramp that are free from contamination of other colored binders.

Spectral Models

Two approaches to spectral modeling will be explored. The first approach employs the use of the Yule-Nielsen Modified Neugebauer model. This model is a commonly known regression-based model used primarily for 2D printing. The second approach utilizes the transparent form of Kubelka Munk Model.

Yule-Nielson Modified Neugebauer

To create a forward model for the printer and binder system, a ramp is created for each binder color for varying percentages of binder coverage. These ramps are then used in combination with the Yule-Nielsen-Murray-Davies equation shown in Eqn. (7) to create a look up table or LUT between RGB digital counts and effective coverage areas. In this equation a_{eff} is the effective dot area, $R_{meas,adj} = R_{meas}^{1/n} - R_s^{1/n}$ and $R_{t,adj} = R_t^{1/n} - R_s^{1/n}$ and where ^{T} and $^{-1}$ represents transpose and inverse respectively. R_{meas} is the measured reflectance of the sample, R_s is the reflectance of the white power, and R_t is the reflectance of the colored binder at 100% coverage, and n is the a parameter accounting for light spreading in the substrate [13].

$$a_{eff} = R_{meas,adj} R_{t,adj}^T \left(R_{t,adj} R_{t,adj}^T \right)^{-1} \qquad (7)$$

To create the LUT, n is optimized by iterating though a range of values and solving Eqn. 7 for an effective area value that minimizes the RMS value between the measured reflectance and the reflectance predicted by substituting a_{eff} into equation 4. . In our case this results in a global n value of 1.13. This results in 30 effective areas, 10 for each binder. The LUT is constructed by performing a cubic spline interpolation between each effective area for each binder. The red digital count is used as the input value for the cyan binder, the green digital count is used for the magenta binder, and the blue digital count is used for the yellow binder.

Using the optimized n value, calculated area coverages, and Eqn. 4, the reflectances of the ramps and the 125 test samples are predicted. The predictions of the ramps are shown in Figures 5, 6, and 7. The predictions for 10 randomly selected test samples are shown in Fig. 8. The top half of each graph represents the measured color, and the bottom half represents the predicted color. The dotted line represents the predicted spectrum, while the solid line represents the measured data. The color differences as calculated by ΔE_{00} are also recorded for each of these patches in Table I. The average ΔE_{00} value of the ramp samples was found to be 1.61. The average ΔE_{00} for the 125 test samples was 9.07.

Althougth the average ΔE_{00} value for the ramp data was less than 2, the overall average for all the test samples was very high. This is not an unexpected performance from this model. The model reasonably predicts reflectance of samples that use only one colored binder but quickly breaks down when used to predict reflectances of binder mixtures, especially mixtures that greatly differ from the ramp data. Because the model performs so poorly when applied to binder mixtures, a second appoarch, a model employing the transparent form of the Kubelka-Munk model, will be explored.
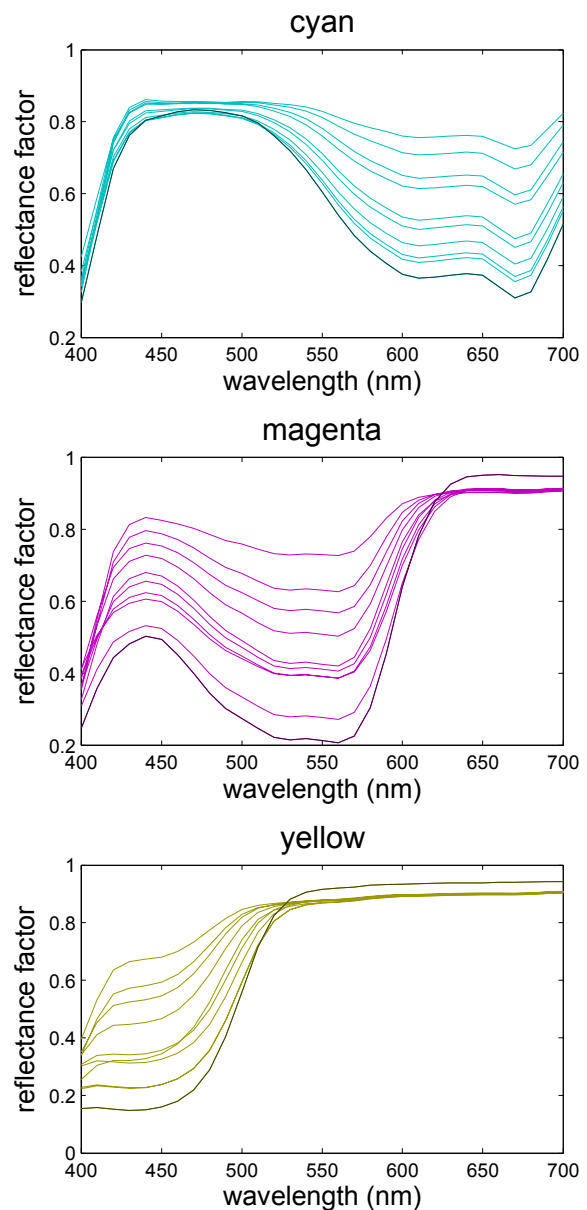

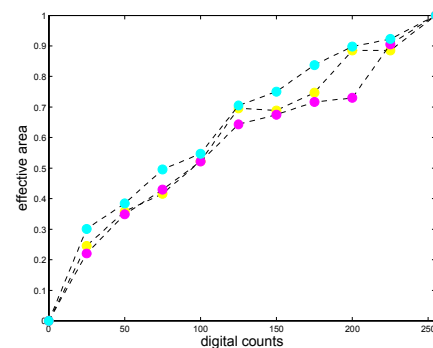**Fig. 3.** *Cyan, magenta, and yellow reflectance factor plots from ramps.*

Fig. 4. *Cyan, magenta, and yellow effective area look up table from RGB digital counts.*
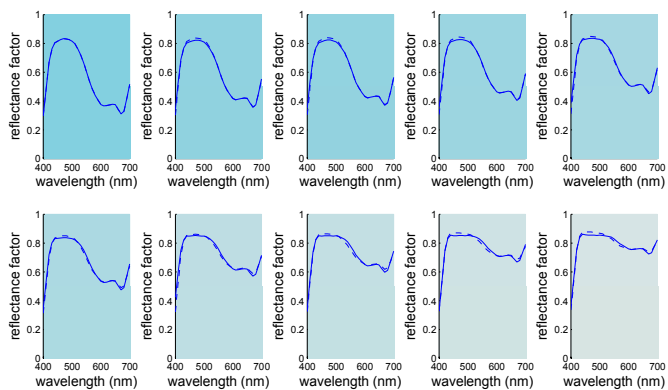
Fig. 5. *Model predicted reflectance factor (dotted) and corrected measured reflectance factor (solid) plotted for each of the 10 samples in the cyan ramp. The top half of each plot represents the measured data in sRGB, and the bottom half represents the predicted data in sRGB*
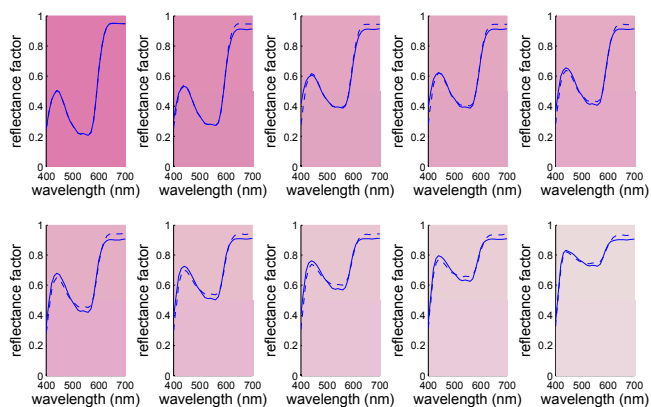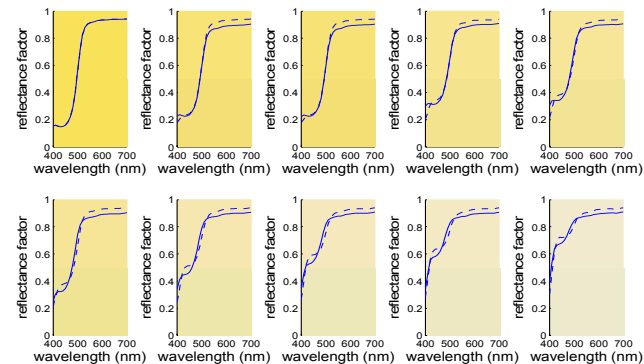

Fig. 6. *Model predicted reflectance factor (dotted) and corrected measured reflectance factor (solid) plotted for each of the 10 samples in the magenta ramp. The top half of each plot represents the measured data in sRGB, and the bottom half represents the predicted data in sRGB.*

Fig. 7. *Model predicted reflectance factor (dotted) and corrected measured reflectance factor (solid) plotted for each of the 10 samples in the yellow* ramp. *The top half of each plot represents the measured data in sRGB, and the bottom half represents the predicted data in sRGB*

Transparent K-M
Part I

The first step in creating the spectral model using transparent form of Kubelka Munk is to convert measured reflectance to absorptance. The conversion is done by first correcting the measured reflectance for

refractive index discontinuity using the Saunderson equation for specular excluded conditions, shown in Eqn. (6) [*11*]. The corrected absorptances of the maximum cyan, magenta, and yellow, samples with digital counts [0 255 255], [255 0 255], and [255 255 0] are shown in Fig. 9.
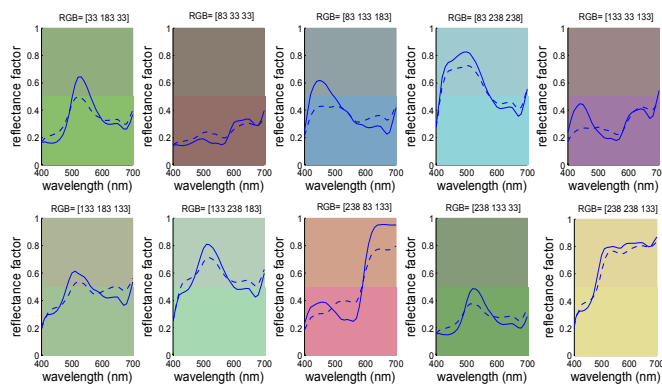

Fig. 8. *Neugebauer model predicted reflectance factor (dotted) and corrected measured reflectance factor (solid) plotted for each of the 10 test samples. The top half of each plot represents the measured data in sRGB, and the bottom half represents the predicted data in sRGB*
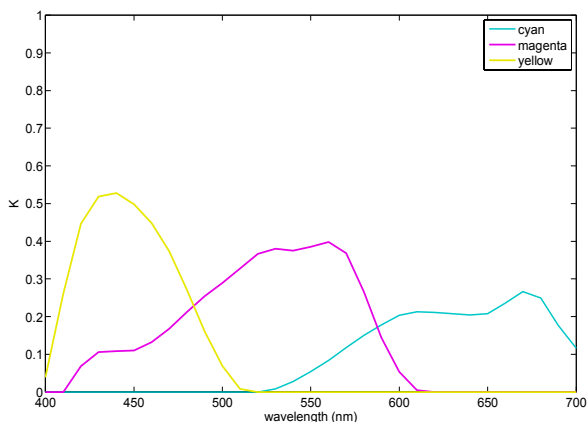

Fig. 9. Cyan, magenta, and yellow absorptance factor versus wavelength.

The second step is to calculate concentration values of ink amounts from the primary ramps using [*11*]:

$$c_c = \frac{\int_\lambda K_{\lambda,cyan}}{\int_\lambda K_{\lambda,cyan\,max}},$$

$$c_m = \frac{\int_\lambda K_{\lambda,magenta}}{\int_\lambda K_{\lambda,magenta\,max}}, \qquad (8)$$

$$c_y = \frac{\int_\lambda K_{\lambda,yellow}}{\int_\lambda K_{\lambda,yellow\,max}},$$

A plot of the concentrations of the cyan, magenta, and yellow binders versus normalized digital counts is shown in Fig. 10.
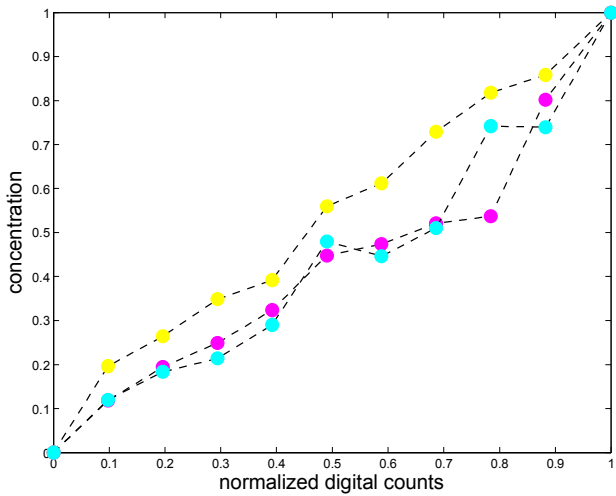

Fig. 10. *Cyan, magenta, and yellow binder concentrations versus normalized digital counts calculated from absorptance data.*

The relationship between concentration and normalized digital counts is not a linear one, therefore a degree 3 polynomial is fit between normalized digital counts and concentrations. This fit is performed by using multi-linear regression *[11]*. The results shown:

$$c_c = 1.07d_c - 0.98d_c^2 + 0.90d_c^3$$
$$c_m = 1.43d_m - 2.16d_m^2 + 1.72d_m^3 \qquad (9)$$
$$c_y = 1.46d_y - 0.99d_y^2 + 0.53d_y^3$$

are used to calculate predicted binder concentrations from normalized digital counts. These concentrations are then used to calculate the absorptance of samples that are made up of a mixture of binders using the following equations *[11]*:

$$K_{\lambda,cyan} = c_c K_{\lambda,cyan,max}$$
$$K_{\lambda,magenta} = c_m K_{\lambda,magenta,max} \qquad (10)$$
$$K_{\lambda,yellow} = c_y K_{\lambda,yellow,max}$$
$$K_{\lambda,mix} = K_{\lambda,cyan} + K_{\lambda,magenta} + K_{\lambda,yellow} \qquad (11)$$

Reflectance factor is then calculated from the calculated K value using Eqn. (10) which is Eqn. (5) rewritten.

$$R_{predicted} = R_{white} * e^{-2K} \qquad (12)$$

In this equation, R_{white} is the reflectance of the white sample, or blank substrate without any binder present *[10]*. An inverse Sanderson is then applied to the calculated reflectance factor values:

$$R_{\lambda,i} = \frac{R_{\lambda,predicted}(1-K_1)(1-K_2)}{(1-K_2)R_{\lambda,predicted}} \qquad (13)$$

Part II

Because of the nonlinear relationship plotted in Fig. 10 a second a method was employed to model calculated

absorptance data. In this method, a spectral matching criteria is used. The intension is to minimize the RMS between predicted and calculated absorptance using *[11]*:

$$c = (\phi'\phi)^{-1}f$$

$$\phi = \begin{bmatrix} K_{\lambda=1,cyan,max} & K_{\lambda=1,magenta,max} & K_{\lambda=1,yellow,max} \\ \vdots & \vdots & \vdots \\ K_{\lambda=n,cyan,max} & K_{\lambda=n,magenta,max} & K_{\lambda=n,yellow,max} \end{bmatrix} \qquad (14)$$

$$f = \begin{bmatrix} K_{\lambda=1,standard} \\ \vdots \\ K_{\lambda=n,standard} \end{bmatrix}, c = \begin{bmatrix} c_c \\ c_m \\ c_y \end{bmatrix}$$

where n is the number of wavelengths in the spectral measurement and c_c, c_m, and c_y are concentration values of cyan, magenta, and yellow ink for any sample, referred to as the standard in the above equation.

The calculated concentration values of the samples and their corresponding normalized digital counts are then related to each other with a degree 3 polynomial by multi-linear regression. The form of the polynomial is:

$$c_c = b_1 + b_2 R + b_3 G + b_4 B + b_5 RR + b_6 GG$$
$$+ b_7 BB + b_8 RG + b_9 RB + b_{10} GB + b_{11} RRR \qquad (15)$$
$$+ b_{12} GGG + b_{13} BBB + b_{14} RGB + b_{15} RRG$$
$$+ b_{16} RRB + b_{17} GGR + b_{18} RBB + b_{19} BBG + b_{20} GGB$$

The equations for the magenta and yellow concentrations are similar, however each of the three polynomials have different coefficients. These calculated coefficients and eqns. 10 through 13 are used to predict reflectance factor values from normalized digital counts.

Samples Used to Test Performance of Model

The first approach to using the absorptance data builds a model from only cyan, magenta, and yellow ramp data. The second approach uses all printed samples, discussed earlier, except 10 samples selected from the 5x5x5 factorial. These are the same 10 samples shown in Table I.

TABLE I.   THE COLOR DIFFERENCE (ΔE_{00}) BETWEEN MEASURED AND PREDICTED REFLECTANCE FACTOR VALUES OF 10 RANDOMLY SELECTED SAMPLES FOR EACH OF THE THREE MODELS

Sample	YNMN	KM Part 1	KM Part 2
1	8.24	9.37	4.15
2	13.06	6.22	6.15
3	10.61	17.07	7.92
4	4.19	8.29	0.58
5	15.35	16.86	2.19
6	7.60	9.82	0.39
7	7.45	9.96	3.16
8	17.74	19.19	2.25
9	9.18	13.85	3.40
10	3.22	5.90	2.79
Average ΔE_{00}	**9.66**	**11.65**	**3.30**

Model Performance

To evaluate the performance of each model, color differences are calculated between the measured reflectance factor values of each tile used to construct the model and the reflectances predicted by the model. The mean, minimum, maximum, and 95th percentile color difference and RMS values are reported in Table II.

The color differences of the patches used to create the model are higher than expected. This could be due to errors introduced by fluorescence, the textured nature of the samples, or specular aspects that are not accounted for by the model. The model results in small RMS errors but large color difference errors. This is expected, because the model uses a spectrally based minimization rather than a colorimetric minimization.

The Kubelka-Munk models are also used to calculate a predicted reflectance value for the 10 samples that were not used in creating the model. Their color difference values are shown in Table II. The predicted and measured reflectance factors of the test samples are plotted in Fig. 11 and 12. Again, the top half of each graph represents the measured color, and the bottom half represents the predicted color. The dotted line represents the predicted spectra, while the solid line represents the measured data with the correction applied. The average color difference for all 10 patches is 11.65 for KM Part 1 and 3.29 for KM Part 2. This is more than visually noticeable for solid color patches. A common rule of thumb for color difference is to have a ΔE_{00} value less than 1.00. In Fig. 11, and Fig. 12 some of the samples with larger ΔE_{00} values have a noticeable visual difference. For example, the second predicted patch has a prediction that contains more red than the measured spectra. In other samples little to no visible differences can be detected. Fig.13 shows all three methods plotted with the measured reflectance factor for visual comparison. It is evident that none of models perform particularly well but the KM Part 2 approach performs better than the other two methods.

Discussion

The use of the transparent form of the Kubelka-Munk theory with Saunderson correction and spectral matching criteria allows for a prediction of printed samples with an average ΔE_{00} value of 3.45 for data used in the model and an average of 3.29 for samples not used to construct the model. These values are high, but still this high color difference could be caused by errors introduced by fluorescence or specular components that were not included in the model but are evident when viewed under magnification as shown in Fig. 2. Fluorescence seems to be a reasonable source of this error because samples with larger amounts of blue, in terms of their spectra, have larger errors than samples with smaller amounts. The blue region of the spectra is where the powder and binder fluoresce.

Although the color difference errors that resulted from the KM approach are higher than desired, they are significantly lower than values that resulted from the Yule-Nielsen modified Neugebauer approach that had an average ΔE_{00} value of 1.61 for samples used to create the model and a ΔE_{00} value of 9.07 for all of the 125 test samples. This large error is attributed to trying to interpolate over the entire gamut of the printer from only 8 primaries. The mean, minimum, maximum and 95th percentile for all samples used to create each model are shown in Table II.
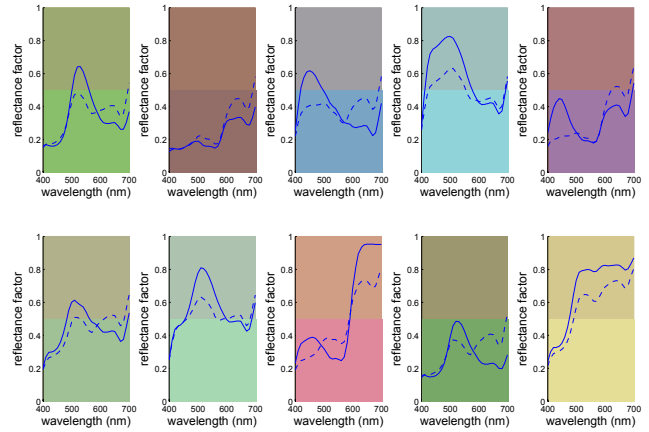

Fig. 11. *KM Part 1 Model predicted reflectance factor (dotted) and corrected measured reflectance factor (solid) plotted for each of the 10 test samples. The top half of each plot represents the measured data in sRGB, and the bottom half represents the predicted data in sRGB*
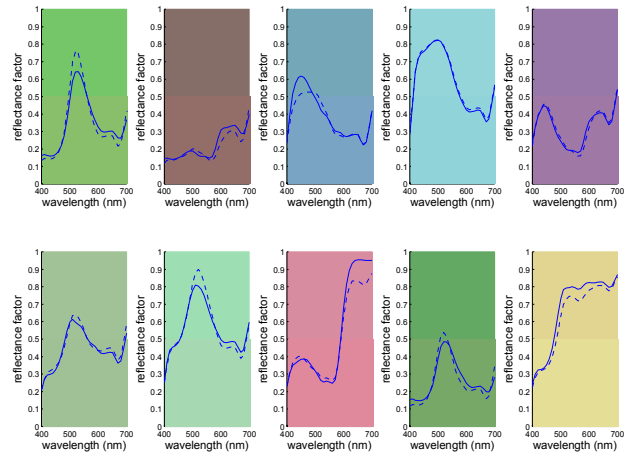

Fig. 12. *KM Part 2 Model predicted reflectance factor (dotted) and corrected measured reflectance factor (solid) plotted for each of the 10 test samples. The top half of each plot represents the measured data in sRGB, and the bottom half represents the predicted data in sRGB*
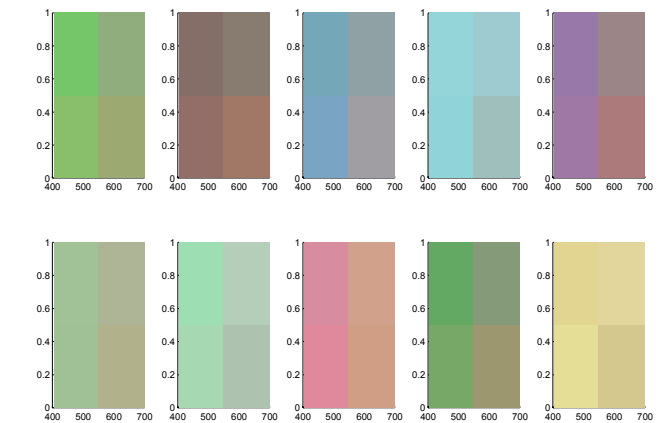

Fig. 13. *All three models visually compared with the measured sample from top left to bottom right: KM Part 2, Yule Nielsen Modified Negebaurer, Measrued Sample and KM part 1.*

TABLE II. PREDICTED VS. MEASURED REFLECTANCE FACTOR FOR 125 SAMPLES FOR ALL THREE METHODS

Method	Metric	Mean	Min	Max	95th Percentile
YNMN	RMS	0.09	0.03	0.13	0.12
	ΔE_{00}	9.07	2.25	21.77	16.40
KM Part1	RMS	0.11	0.035	0.17	0.16
	ΔE_{00}	12.27	3.84	35.64	19.19
KM Part 2	RMS	0.037	0.011	0.16	0.07
	ΔE_{00}	3.45	0.39	17.85	7.84

Conclusions and Future Work

3D printing is a rapidly emerging technology and little is known about color production processes in these devices. In this paper we have attempted to characterize a commercial 3D printer using two standard models. The results represent a meaningful first step, but complexities in the hardware, software, and media seem to require more sophisticated models. Future work could take several directions. First, Kubelka-Munk theory is not typically used for inks and printers, although it has shown to be successful in some cases [10]. A more traditional and accepted approach to modeling printers is the use of the Neugebauer theory. Future work could include reprinting samples that could be used to test the Cellular Neugebauer approach, reviewed by Wyble and Berns in 2000, with appropriate corrections and additions, and compare it to the approaches described above [9]. Of additional interest would be the creation of an inverse model that would take in desired CIELAB values and predict RGB digital counts to be used by the printer to reproduce the color. In fact, a solution to this problem is arguably more important than the forward model.

There is still much work to be done, but the promise of full-color 3D printing in the areas of rapid prototyping, individualized manufacturing, and product customization should serve as sufficient motivation for the required efforts.

Acknowledgments

References

[1] Bill Bumgarner, "Getting Started with a 3D Printer," pp. 12-22, 2013.

[2] 3D Systems. (2013) Freshfiber. [Online]. http://www.freshfiber.com/name-melt/

[3] 3Ders. (2011) 3Ders: 3D Printers and 3D Printing News. [Online]. http://www.3ders.org/3d-printing/3d-printing-history.html

[4] Charles Hull, "Apparatus for Production of Three-Dimensioanl Objects by Stereolithography," Utility 4575330, March 11, 1986.

[5] Solid Concepts Inc. (2009, January) Solid Concepts. [Online]. https://www.solidconcepts.com/content/pdfs/brochures/selective-laser-sintering-sls-brochure.pdf

[6] Summary Corporation. (2011) RPWorld Rapid Prototyping and Manufactruing. [Online]. http://rpworld.net/cms/index.php/additive-manufacturing/rp-rapid-prototyping/fdm-fused-deposition-modeling-.html

[7] Z Corportation, Spectrum Z510 3D Printer Hardware Manual, August 2007.

[8] Maja Stanic, Branka Lozo, and Diana Gregor Svetec, "Colorimetric properties and stability of 3D prints," *Rapid Prototyping Journal*, vol. 18, no. 2, pp. 120-128, 2012.

[9] David R., Berns, Roy S. Wyble, "A Crititical Review of Spectral Models Applied to Binary Color Printing," *Color Research and Application*, vol. 25, no. 1, pp. 4-19, February 2000.

[10] D. Tzeng and R. S. Berns, "A Review of Principal Component Analysis and Its Applications to Color Technology," *COLOR Research and Application*, vol. 30, no. 2, pp. 84-98, April 2005.

[11] Roy S. Berns, "Spectral Modeling of a Dye Diffusion Thermal Transfer Printer," *Journal of Electronic Imaging*, vol. 2, no. 4, pp. 359-370, October 1993.

[12] Roger P. Best, "Computer Match Prediction-Pigments," in *Colour Physics for Industdry*. West Yorksire, England: Society of Dyers and Colourists, 1987, pp. 186-210.

[13] David R. Wyble, "A Critical Review of Spectral Models Applied to Binary Color Printing," *Color Research and Applicatoin*, vol. 25, no. 1, pp. 4-19, February 2000.

[14] J-P. Kruth, P. Mercelis, J. Van Vaerenbergh, L. Froyen, and M. Rombaut, "Binding Mechanisms in Selective Laser Sintering and Selective Laser Melting," *Rapid Prototyping Journal*, vol. 11, no. 1, pp. 26-36, 2005.